

# EFFECT OF OXIDE LAYER THICKNESS ON THE POOL BOILING CRITICAL HEAT FLUX OF PRE-OXIDIZED RPV MATERIAL

H. H. Son, U. Jeong, G. H. Seo, G. Jeun and S. J. Kim\*

Department of Nuclear Engineering, Hanyang University  
222 Wangsimni-ro, Seongdong-gu, Seoul, 133-791, Republic of Korea  
hhson@hanyang.ac.kr; ujeong@hanyang.ac.kr; seokh@hanyang.ac.kr;  
thlab@hanyang.ac.kr; sungjkim@hanyang.ac.kr

## ABSTRACT

For successful execution of the In-Vessel Retention (IVR) and External Reactor Vessel Cooling (ERVC) strategy, defining the Critical Heat Flux (CHF) on the outer surface of the Reactor Pressure Vessel (RPV) is a key objective to secure the thermal integrity of the RPV. Since the CHF is strongly affected by surface conditions of the heating material, if any surface treatments are not applied to the RPV outer surface, corrosion can govern the effects on the CHF. Note that natural corrosion occurs continuously for long time on the RPV. In this regard, pool boiling heat transfer experiment under atmospheric pressure with deionized water was conducted with the pre-oxidized RPV material, whose grade is SA508. The CHF of the bare SA508 increased by 1.5 times, as the heating surface is gradually oxidized approaching the CHF. As a result, it became hydrophilic and nano-porous with the formation of magnetite nanoparticles during nucleate boiling. When the SA508 was pre-oxidized at 300 °C in dry air, however, the CHF was deteriorated even though the oxidized surface was still hydrophilic. Considering that the thermal properties of the pre-oxidized surface experiences some changes as the crystallized oxide layer forms with the specific thickness, the thermal effusivity of magnetite layer is lowered by 0.28 times than that of the bare SA508. Based on the thermal activity-based theory, it may disseminate the effect of lateral heat dissipation, subsequently promotes local dry spot. Consequently, the oxidation behavior of the RPV shows some potential in generating adverse effect on the CHF.

## KEYWORDS

Critical Heat Flux, Oxidation, Oxide layer thickness, IVR-ERVC

## 1. INTRODUCTION

As a practical remedy for the severe accident management, In-Vessel Retention (IVR) strategy has been proposed to maintain mechanical integrity of the Reactor Pressure Vessel (RPV). Major IVR strategies include steam generator feedwater injection, reactor coolant system (RCS) depressurization, steam generator feedwater injection, and containment coolant injection, all of which are prescribed in the severe accident management guidance (SAMG) as Mitigations 1, 2, 3, and 4, respectively. Among these, containment coolant injection plays an important role in cooling down molten corium outside the RPV, and removing decay heat to acceptable level for maintaining long-term cooling. If sufficient amount of cooling is not provided, it promotes the formation of vapor film on the RPV surface, and, in turn, the trapped heat within the vapor film rapidly raises temperature of the RPV outer surface. Under this condition, Critical Heat Flux (CHF) occurs and it may cause the RPV failure by weakening its mechanical strength [1]. In this

---

\* Corresponding author: Tel: +82-2-2220-2355, Email: sungjkim@hanyang.ac.kr

regards, securing the sufficient coolability without occurrence of the CHF is essential to retain integrity of the RPV and related studies have been performed by many researchers [1-4].

In situation of the IVR-ERVC, the coolability limit is determined by the total decay heat of molten corium transferred toward the RPV outer surface. However, molten corium consists of metallic and oxidic layer and its relocation pattern is very uncertain depending on the accident types and sequences. For example, if the thinner metallic layer is formed on the top of the molten corium, the more heat is transferred through the near-vertical wall of the RPV, which, in turn, promotes the occurrence of the CHF. Such process is called as focusing effect [1]. Thus, it is challenging to define accurate coolability limit for the IVR-ERVC strategy due to the diverse locations of the CHF coupled with the accident progression.

In this regard, many researchers have attempted to enhance the CHF on the RPV outer surface using nanofluids or surface coating techniques. Recently nanofluids have received attention as an effective way to enhance the CHF. In the birth of the nanofluids concept, Choi introduced a method to increase the thermal conductivity of heat transfer fluid, in single-phase, using highly conductive nanoparticles [5]. In connection with boiling heat transfer application, Kim et al. showed that liquid microlayer evaporation induces the subsequent deposition of nanoparticles, which forms porous layer on the boiled surface. After nanoparticle deposition, the CHF was enhanced up to 80% with silica nanofluids and the attributed reason was the improved wettability coupled with porous layer [6]. In addition to Kim et al.'s study, Kim and Kim insisted that the CHF enhancement in nanofluids depends on not only the improved wettability but also the capillarity, which effectively promotes liquid supply into dry patch [7].

Besides nanofluids, surface coating is also considered as a promising method to enhance the CHF. Among many surface coating techniques, micro-porous coating is recognized as the most effective technique to enhance the CHF because porous structure includes many capillary channels on the heating surface and helps break up vapor films. Yang et al. conducted flow boiling CHF experiments, using small-scaled test vessel, to investigate the effect of micro-porous aluminum coating on the CHF. In all angles of the lower head, the CHF was enhanced by approximately 2 times and the maximum CHF enhancement occurred in the bottom center. As well, the durability of aluminum coating was confirmed in many cycles of steady-state boiling [8]. Moreover, in order to facilitate the surface coating in an engineering scale, Seo et al. used Single Walled Carbon Nano Tube (SWCNT) coating technique on the SS316 heater specimen. CNT coating process is relatively simple and cost-effective compared to other techniques because the fabrication is conducted at room temperature condition. They showed that the CHF was enhanced by 1.5 times with the maximum coating thickness of 1 $\mu$ m even though nucleate boiling heat transfer coefficient was reduced by half [9].

The applicability of these techniques left some future works because the effect of material aging was not addressed properly. As a matter of fact, when the RPV made of low carbon steel alloy of SA508 is used, the aging issue becomes critical because the SA508 is highly corrosive material due to its low chromium concentration of 0.25wt.%. Theofanous et al. reported that for the near vertical wall the fully-aged CHF value of  $\sim 1.6$  MW/m<sup>2</sup> is higher than the initial value of  $\sim 1.2$  MW/m<sup>2</sup> [1]. It implies that surface aging effect in the IVR-ERVC application causes considerable discrepancy in predicting the CHF. Furthermore, in order to investigate the surface aging effect on the CHF, Lee and Chang conducted pool boiling CHF experiment with the SA508 using nanofluids with the suspensions of Al<sub>2</sub>O<sub>3</sub> and CNT. Then, the CHF was enhanced by 68% when boiled for longer than 50 minutes without any additives. They insisted that the reason for the CHF enhancement was due to magnetite nanoparticle deposition, which makes the surface hydrophilic [10]. Interestingly, however, the CHF of the oxidized SA508 was barely affected by the nanofluids. It indicates that the advantage of nanofluid for the CHF enhancement fade away when the heating surface is easily oxidized during nucleate boiling. Likewise, under the flow boiling condition, DeWitt et al. confirmed the existence of textured oxide layer through SEM image on the surface of the SA508 before the occurrence of CHF. They also showed no significant effect of nanofluids with the SA508 [11]. These studies focused on the surface change only during nucleate boiling, which may imply that the heating surface is clean before initiation of nucleate boiling.

It was noticed that those aforementioned studies deal with the fast corrosion during operation. The rationale behind the study could be assuming that the RPV outer surface will be clean when the IVR-ERVC initiates.

However, the RPV is an irreplaceable component for lifetime of Nuclear Power Plant (NPP), and thus, it will continuously experience natural corrosion for a few decades. On the basis of the western Pressurized Water-cooled Reactor (PWR), aging management to minimize corrosion of the RPV has been focused on the inner region in contact with coolant. Inner surface of the RPV is covered by a clad of austenitic stainless steel inducing galvanic corrosion. The RPV outer surface is exposed to the normal PWR operating temperature of 285 to 320 °C without any treatments. Generally, the corrosion rate of low carbon steel in the industrial condition reaches  $0.025 \text{ mm}\cdot\text{yr}^{-1}$  [12]. In specific, Sakai et al. showed that the oxidation kinetics of pure iron follows a parabolic rate law and the oxide layer thickness increases by 100 nm for a day at 300 °C in air [13]. In addition, Bertrand et al. found the parabolic rate constant of pure iron, which is  $4.1\times 10^{-9} \text{ mg}^2\text{cm}^{-4}\text{s}^{-1}$  at 300 °C in synthetic dry air, is in good agreement with the Sakai et al.'s data [14]. These literatures suggest that the oxide layer thickness of the SA508 will range from dozens to hundreds of microscale for lifetime of the NPP. Given that the surface characteristics effective to boiling heat transfer are defined in micro/nanoscale (i.e. wettability, roughness, capillarity, cavity density, and surface factor), it is inevitable to reflect the effect of oxide layer thickness including the surface characteristics on the CHF. In this regard, an objective of present study is to evaluate the effect of pre-oxidation of the SA508 on the CHF. The pool boiling CHF experiment was conducted with the pre-oxidized SA508 under atmospheric pressure with deionized water. The oxidation treatment on the SA508 was carried out in the laboratory furnace and the resultant thickness of oxide layer was estimated by measuring the mass gain along with the oxidation time. Since the oxidation changes the surface characteristics with aspect of physical and chemical, the contact angle and the roughness were carefully quantified. However porosity of the pre-oxidized SA508 was not considered in this study because the temperature condition of 300 °C is too low to develop the porous media [15]. Especially, at the interest of the effect of oxidation state on the CHF, the fundamental differences of the CHF mechanisms between the bare and the pre-oxidized SA508 were discussed in detail.

## **2. CHARACTERISTICS OF OXIDIZED SURFACE**

As an effort to address aging issue of metals and alloys, many researchers have revealed that the oxidation behavior of pure iron and iron-based alloy changes the mechanical, physical, and chemical properties of material. Especially, in boiling heat transfer application using high power density, the oxidation or fouling is related to its thermal efficiency and safety because the changed surface characteristics affect dominantly boiling heat transfer capability. Since the SA508 is also iron-based alloy, understanding how the oxide structure develops on the surface is essential to figure out the relationship between the oxidation behavior and the CHF mechanism.

Once the iron-based alloy is oxidized, chemical composition within surface structure is changed to ceramic series whose elements are iron oxides. Many literatures reports that the iron oxides develop the crystallized structure, individually aligned, such as hematite ( $\text{Fe}_2\text{O}_3$ ), magnetite ( $\text{Fe}_3\text{O}_4$ ), and wustite ( $\text{FeO}$ ). Among these, wustite is thermodynamically unstable below 575 °C, whereas hematite and magnetite phases are stable in the most temperature range [14, 16]. Hussey et al. investigated the thickness ratio of hematite to magnetite and concluded that magnetite layer is much thicker than hematite layer [17]. Additionally, in the study of dry corrosion of low-alloyed steel in low temperatures between 260 and 500 °C, Bertrand et al. showed that the thickness ratio of magnetite is above 95% along the oxide scale at the targeted temperature range [14]. Thus, it is well addressed that the entire oxide structure of low-alloyed steel such as SA508 will be composed of almost magnetite layer because the RPV is exposed to the normal PWR operating temperature of 285 - 320 °C for lifetime.

### **2.1 Surface structure of oxidized SA508**

In this study, the magnetite layer formed on the pre-oxidized SA508 was confirmed by elementary analysis using Energy Dispersive Spectroscopy (EDS) technique. The EDS detector is capable of distinguishing

various energy spectrums from characteristic X-ray emitted by each atom on the target surface. Since the magnetite is composed of two atoms, Fe and O, it is easily confirmed that there exists magnetite layer by detecting the energy peak of Fe and O. In Fig. 1(a), the atomic ratio of Fe and O was specified with respect to the oxidation time. In the bare specimen, oxygen concentration on the surface is measured approximately 7.4 at.% and this low value indicates that the clean surface is almost oxygen free. Once the surface was oxidized, however, the oxygen concentration highly increased up to 50 at.% although some discrepancy exists due to measurement error. After oxidation, the summation of atomic percent of Fe and O is approximately 90%. In this regards, the target layer is deemed to be made of magnetite alone.

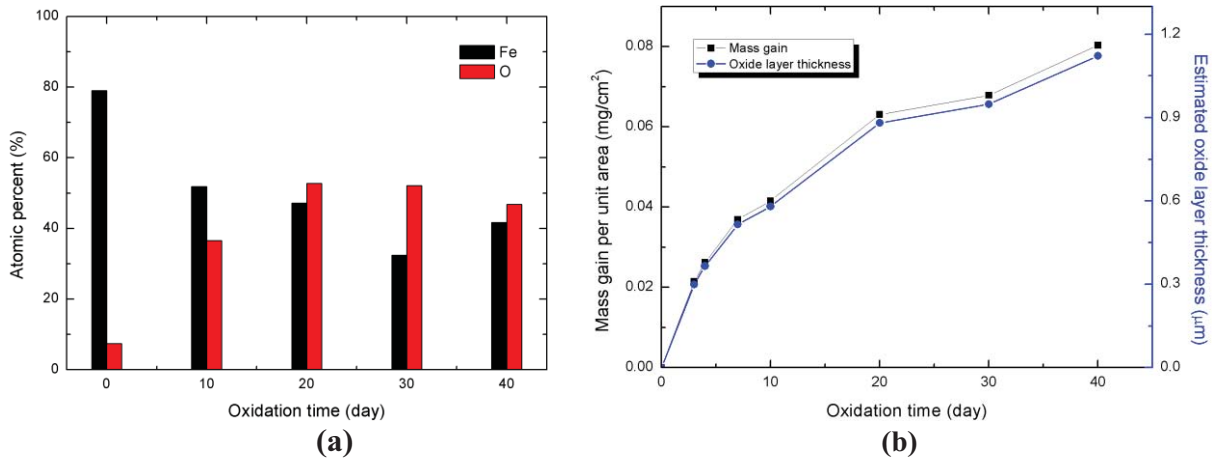


**Figure 1. (a) Elementary analysis for confirmation of chemical composition on the oxidized surface and (b) growth of oxide scale in SA508.**

For the purpose of evaluating a dependency of the oxide layer thickness on the CHF, the scale growth of the SA508 was estimated by measuring the mass gain at oxidation time of 3, 10, 20, 30, and 40 days under the condition of 300 °C in dry air. The mass gain data was converted to the oxide layer thickness,  $x$ , using following equation:

$$x = \left( \frac{\Delta m}{A} \right) \left( \frac{1}{\rho_{ox}} \right) \left( \frac{M_{ox}}{M_{O_2}} \right) \quad (1)$$

where  $\rho_{ox}$  is the density of oxide product,  $M_{ox}$  is the molar weight of oxide product, and  $M_{Oxygen}$  is the molar weight of oxygen. This conversion process assumes that the oxide layer is perfectly compact, thus, the real thickness which perhaps involves pores will be higher than the estimated thickness. Nevertheless, use of the estimated thickness seems to be allowable because the oxide layer consists hardly of the porous media in low temperature (300 °C) and dry air [15]. Both the mass gain and the oxide layer thickness versus oxidation time are plotted in Fig. 1(b).

As reported in the last decade, hydrophilic micro/nanostructures on the surface can cause capillary wicking near the CHF [7, 18, 19]. In this study, the surface structure of pre-oxidized SA508 examined by SEM images is shown in Fig. 2. Definitely, the oxide structure as a shape of nanoparticle smaller than 50 nm is constructed and covers over the surface uniformly. In accordance with oxidation time, some difference between oxidized samples was observed. During short-term oxidation in 10 days, only the magnetite nanoparticles were stacked on the upmost surface, whereas in more oxidized surfaces in 20 days, subsequent whiskers as a shape of needle grew on the earlier-formed-magnetite. Based on TEM observations, Bertrand et al. revealed that the whiskers consist of alpha-hematite [14]. In Li et al.'s study, the hematite nanoflake

film is likewise formed in low temperature (375 - 450 °C) [20]. Similar to those of results, the whiskers developed the micro/nanostructure randomly over the surface.

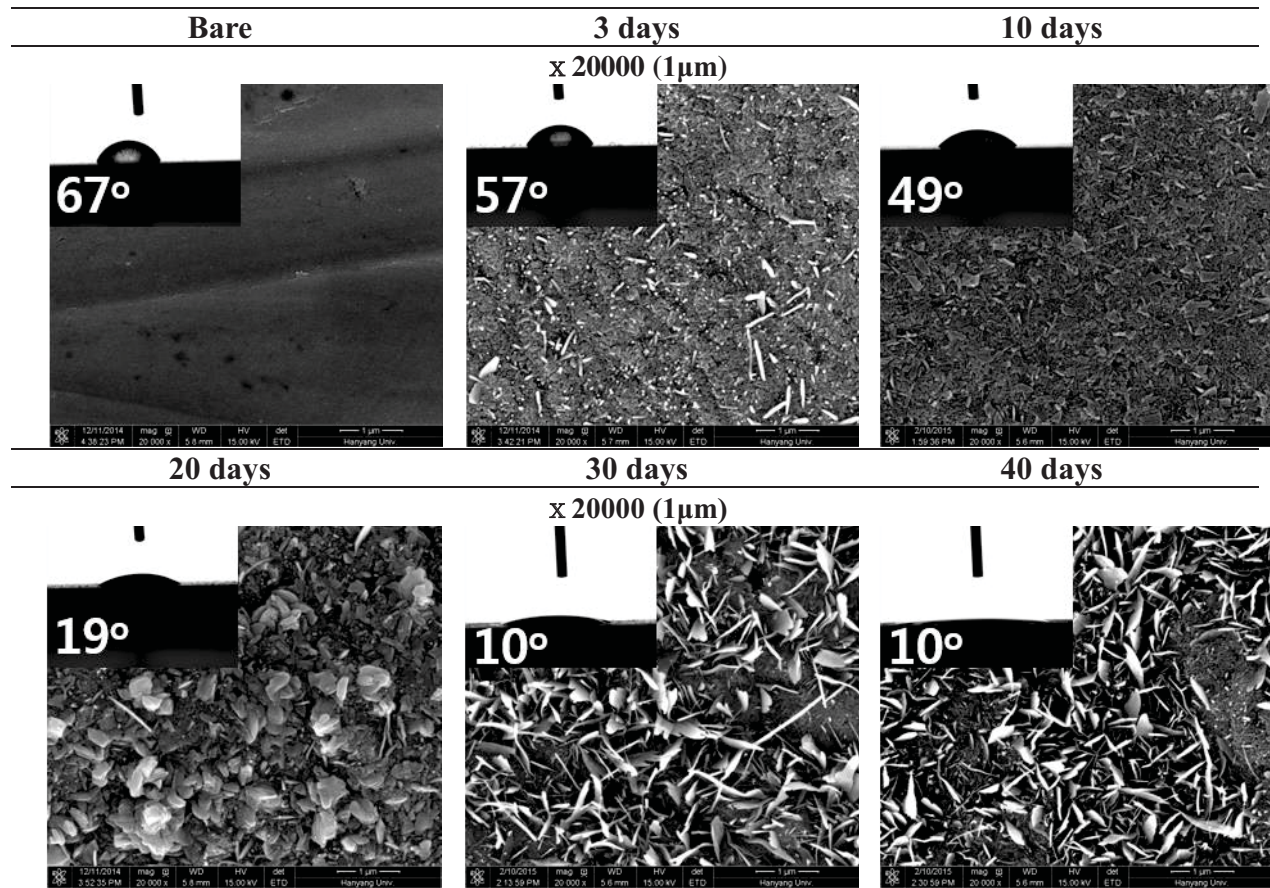


Figure 2. SEM image of pre-oxidized SA508.

## 2.2 Change of wettability with roughness

For the past a few decades, surface wettability has been considered as a key parameter to determine CHF [6, 21]. In general, it is represented by contact angle between solid and liquid. Therefore wettability effect on the CHF is easily quantified by measuring the contact angle. It is known that the contact angle is determined by various surface conditions such as free energy of solid-fluid interface, roughness, capillarity, etc [7, 22, 23]. These parameters play an important role to nexus the relationship between the oxidation and the contact angle. Gomez et al. reported that the contact angle of magnetite as a type of particle is about 37° corresponding to the surface free energy of 48.9 mN/m [24]. In terms of the effect of oxide structure on the contact angle, Oshida et al. showed that the contact angle of pre-oxidized surface decreases, and especially liquid spreading occurs in the cubic structure as the spinel type [25]. The effect of surface roughness on contact angle was investigated by Kim et al. using the modified Young's equation, referred to the Wenzel's model. They proposed that oxide nanoparticles deposited on the heating surface promotes an increase of adhesion tension and effective surface area, accordingly decreases apparent contact angle [6]. To explain the additional enhancement of rewetting capillarity in the contact angle near 0°, Kim and Kim suggested that an increase of the effective contact area induces more capillarity triggering liquid spreading in the

lateral direction [7]. In the same manner, Ahn et al. revealed that highly anodized surface of zircaloy-4 promotes liquid spreading below the contact angle of  $10^\circ$  by help of capillary wicking [18].

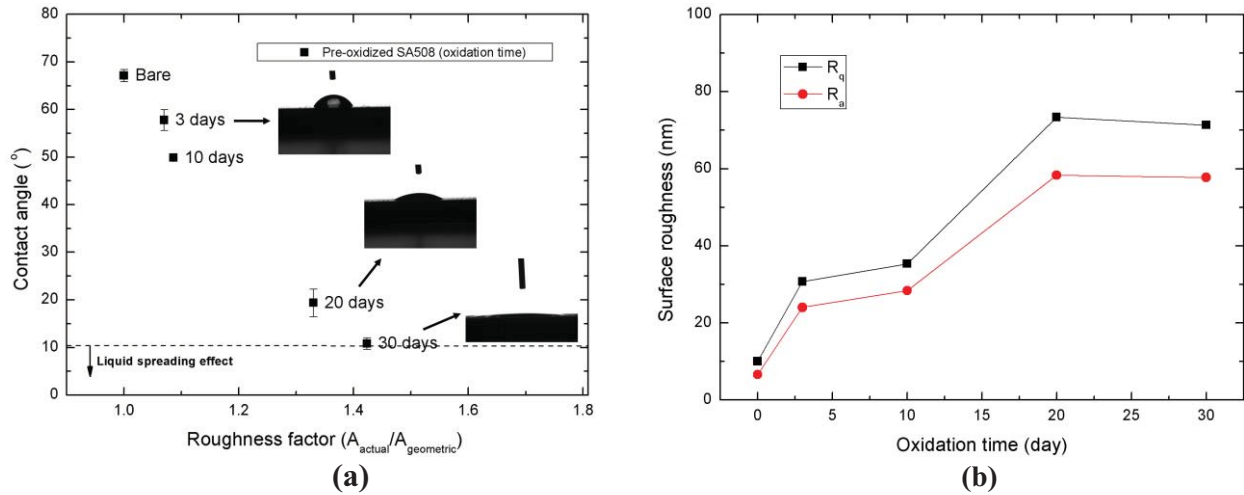


Figure 3. Change of (a) contact angle and (b) roughness along oxidation time.

Based on many studies, the variation of contact angle along oxidation time can be physically understood as follows. Fig. 3(a) represents the change of static contact angle in accordance with roughness factor. The contact angles were measured in room temperature and averaged within an error of  $\pm 3\%$  for three measurements. Obviously, the contact angle decreases gradually as oxidation time increases and eventually reaches to non-equilibrium state after oxidation time of 30 days. In equilibrium state before oxidation time of 30 days, the decreasing trend of contact angle can be qualitatively explained by the effect of roughness factor,  $r$ , defined as the ratio of actual surface to geometric surface. The following expression of Wenzel's model shows the dependency of the roughness factor on the apparent contact angle denoted as  $\theta^*$ :

$$\cos \theta^* = \frac{\gamma_{SV} - \gamma_{SL}}{\gamma_{LV}} r \quad (2)$$

Where  $\gamma_{SL} - \gamma_{SV}$  is the adhesion tension and  $\gamma_{LV}$  is the surface tension. When the rough surface ( $r > 1$ ) is given, this relationship signifies that the apparent contact angle increases with roughness factor if the surface is hydrophobic, whereas the trend is reversed on the hydrophilic surface. As mentioned above, since the surface free energy of magnetite is higher than that of bare surface, the surface of oxidized SA508 is hydrophilic [24]. Considering that the roughness factor increases with oxidation time, therefore, the trend of Fig. 3(a) agrees with Wenzel's model qualitatively. This trend is well understood by the study of Kim et al. explaining that the contact angle decreases on the heating surface, which is covered by oxide nanoparticles, due to an increase of adhesion tension and surface roughness [6].

Beyond the equilibrium state, droplet starts to spread over the surface. In this study, only small spreading was observed on the oxidized surface above 30 days. Then, the criterion of spreading contact angle was about  $10^\circ$ , which is well-matched with the value of Ahn et al. [18]. This liquid spreading effect seems to occur due to lateral capillary wicking within porous media consisting of dense whiskers (Fig. 2). Evidently, the CHF can be improved on the hydrophilic surface coupled with the existence of porous media [7, 19].

The surface roughness was measured by Atomic Force Microscope (AFM) and the tendency versus oxidation time plotted in Fig. 3(b). In present data, the roughness increased by approximately 70 nm as approaching to oxidation time of 30 days. As a matter of fact, this slight change of roughness by oxidation

is hardly effective to the CHF. Kang reported that as the surface is rougher in dozens of nanoscale, more cavity helps to enhance nucleate heat transfer capability with improvement of bubble growth and agitation in low heat flux. But as heat flux increases, this effect fades out because liquid agitation becomes weak in forming vapor slugs [26]. Furthermore, O'Hanley et al. investigated the separate effect of surface roughness on the CHF, maintaining both wettability and porosity the same. Although the average roughness changed from 0.01 to 4 $\mu$ m, its effect on the CHF was hardly observed for the given wettability and porosity [19].

### 3. EXPERIMENTAL DESCRIPTION

#### 3.1. Design of test section

In this study, the test specimen was heated using a DC power supply via copper electrodes connected to each end side of the test specimen. In order to measure the inner surface temperature opposite to the heat transfer surface and voltage drop along the test specimen, a K-type thermocouple and a pair of voltage tap were attached to the end side of the test specimen. The test specimen was made of SA508 Grade 3 Class 1 and designed as a type of straight plate. The length, width, and thickness are set to 42, 10, and 2 mm respectively. The electrical contact between heating material and copper electrode was secured by tightening the end side of heating material using PEEK cover on the copper electrode. In addition, thermal insulation was applied to minimize heat loss through the back and lateral sides of the test specimen using liquid epoxy, which is solidified after mixed with powder. Insulated thickness is 20 mm in the back side and 10 mm in the lateral side.

#### 3.2. Experimental procedures

Experimental procedure with SS316 heaters follows two major steps. Firstly, saturated temperature at atmospheric pressure was achieved using the preheaters equipped in the isothermal bath. To remove non-condensable gas affecting bubble dynamics, saturated state was maintained for approximately one hour. Secondly, power input was increased in step of 40 kW/m<sup>2</sup> until the heat flux reached 70% of the predicted CHF. Closed to the CHF, a smaller heat flux of 20 kW/m<sup>2</sup> was applied to prevent sudden vapor film formation. In each heat flux application, steady state was maintained for at least two minutes while steady wall temperature readings are confirmed. The CHF was determined when inner wall temperature jumped rapidly more than 200 °C. Applied heat flux was calculated using Joule's equation as shown in Eq. (3).

$$q'' = \frac{\text{Power}}{A_{\text{heated}}} = \frac{VI}{WL} \quad (3)$$

where  $V$  is voltage drop at the heating material,  $I$  is current,  $W$  is width of heat transfer area,  $L$  is length of heat transfer area. Voltage drop was measured in each end side of heat transfer area to remove unintended heat loss. Measurement uncertainty was measured using a propagation of error method. The uncertainties on the current ( $U_I/I$ ), voltage ( $U_V/V$ ), and heated length ( $U_L/L$ ) and width ( $U_W/W$ ) values were less than 0.5, 0.5, 2.5, and 0.8 %, respectively. The final measurement uncertainty calculation of 5.2 % was evaluated.

### 4. RESULTS AND DISCUSSION

CHF experiments were carried out for horizontal plate heaters under the condition of saturated water at atmospheric pressure. In table I, each CHF test was classified with oxidation time. Test materials employed are SS316 and SA508. In fact, it is obvious that the boiled surface conditions would be changed by contact with saturated water during nucleate boiling. However, the extent of oxidation formed during the boiling test is definitely different depending on chromium composition of different alloy types. Since the SS316

heater contains high chromium concentration corresponding to 16 wt.%, which is capable of producing passive protection layer for preventing the formation of iron oxide products, the surface change during the boiling test can be ignored. In flow boiling experiment, DeWitt et al. identified that the surface morphology of SS316L are the same regardless of the boiling time [11]. This indicates that the CHF is independent of the boiling time when the chromium concentration of the heating material is sufficiently high.

**Table I. Test matrix for pool boiling CHF test**

Test material	Oxidation temperature (°C)	Oxidation time (day)	Boiling time (min.)	CHF (kW/m <sup>2</sup> )
SS316	No oxidation	0	60	1059 ± 41
		0		1541 ± 8
		3		743 ± 66
SA508	300	10	30	838 ± 25
		20		729 ± 104
		30		792 ± 67
		40		841 ± 93

Unlike SS316, boiling time may act as a significant factor in determining the CHF of SA508 because its corrosive property promotes deformation of the heating surface characteristics during nucleate boiling. Regarding the relationship between the CHF of SA508 and boiling time, Lee et al. reported that the CHF of SA508 increases gradually with boiling time due to the formation of magnetite nanoparticles by water oxidation [10]. In this manner, boiling time of the tested SA508 was set to about 30 minutes, but some variation existed due to difficulty of controlling experimental time from ONB to CHF. The error in each CHF test was higher in SA508 than SS316. It seems that the surface change of SA508 during nucleate boiling is uncertain in accordance with boiling time, thus, hardly regulates the consistency of surface characteristics with the variation of boiling time.

#### 4.1 Effect of wettability on oxidized surface

Fig. 4(a) shows the CHF variation along oxidation time for each test material. The CHF data are spread over the degree of oxidation. In case of SS316 whose surface is not changed during boiling test, the CHF of bare surface occurred at 1037 kW/m<sup>2</sup>, which is in good agreement with Zuber's CHF prediction of 1107 kW/m<sup>2</sup> within error of 6.4 %. Zuber's CHF value was predicted by following equation based on the theory for hydrodynamic instability [27].

$$q_c'' = \frac{\pi}{24} h_{fg} \rho_v^{0.5} [g \sigma (\rho_l - \rho_v)]^{0.25} \quad (4)$$

where  $h_{fg}$  is the enthalpy of vaporization,  $\rho_g$  is the gas density,  $\rho_f$  is the liquid density, and  $\sigma$  is the surface tension of liquid,  $g$  is the gravitational constant. On the other hand, the CHF of bare SA508 occurred at 1541 kW/m<sup>2</sup>. Furthermore, the CHF of all pre-oxidized SA508s was lower than Zuber's value of 1107 kW/m<sup>2</sup>. This result is not consistent with Zuber's hydrodynamic instability theory because he did not consider surface characteristics at all. In terms of wettability effect on the CHF, the mechanistic relationship between the CHF and the contact angle denoted as  $\beta$  was proposed by Kandlikar's CHF model as follows [21]:

$$q_c'' = h_{fg} \rho_g^{1/2} \left( \frac{1 + \cos \beta}{16} \right) \left[ \frac{2}{\pi} + \frac{\pi}{4} (1 + \cos \beta) \cos \phi \right]^{1/2} \times \left[ \sigma g (\rho_l - \rho_g) \right]^{1/4} \quad (5)$$

In this model, surface tension force combined with the contact angle at the bubble base develops anti-force to evaporating momentum. At high evaporation rate near the CHF, evaporating momentum becomes larger than the sum of gravitational and surface tension forces and consequently causes the CHF. Based on force balance, the surface tension force coupled with the contact angle is the only factor delaying the CHF condition. Then, the evaporating momentum can be suppressed by enhancing the surface tension force. However, this result did not agree with his model as ever (Fig. 4(b)), nevertheless the contact angle increases gradually in accordance with oxidation time (Fig. 3(a)). Considering that the SA508 is highly corrosive material, the heating surface can be easily changed in boiled water [10]. Thus, the surface characteristics after nucleate boiling need to be carefully re-evaluated. Fig. 5 shows the surface change of SA508 after nucleate boiling of 30 minutes without burnout of the boiled surface. Noticeably, in the bare SA508, many oxide products were deposited on the heating surface, not shown before boiling experiment (Fig. 2). In the EDS analysis, it was observed that these oxide products consist of iron (Fe) and oxygen (O) with the atomic percent of 76 and 23, respectively. Thus, these particles with the size of 60-140 nm are a series of iron oxide. Moreover, the spherical-shaped particles seem to make nano-porous structure over the surface. These nanoparticles regarded as a type of magnetite which are chemically hydrophilic, and possibly enhance the CHF with nano-porous structure. The result for the CHF of the bare SA508 is consistent with the studies conducted in KAIST [10, 28]. Lee and Chang insisted that the CHF behavior of the bare SA508 is similar to the case in use of nanofluid with suspension of magnetite nanoparticle making the boiled surface wettable. In fact, the deposition of magnetite nanoparticle on the heating surface improves wettability capable of enhancing rewetting effect near the CHF [10]. However, this effect appears hardly in the pre-oxidized SA508. As shown in Fig. 4(a), the CHF of pre-oxidized SA508 is always lower than Zuber's CHF value even though the surface is hydrophilic. Similar results for the effect of the CHF deterioration on surface aging were summarized in the report of G. R. Beitel. A few results suggested that surface aging increased the wall superheat in pool boiling system, moreover, the CHF with the presence of ferric-oxide scale and aluminum oxide coating decreased [29].

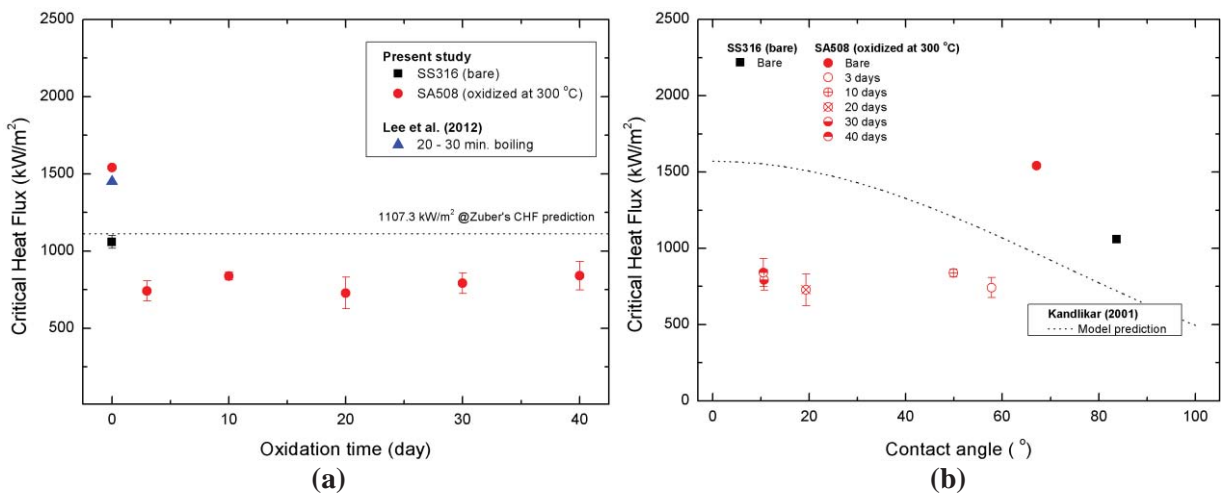
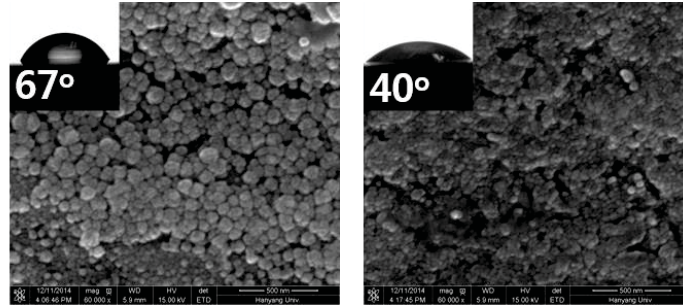


Figure 4. CHF variation of the SS316 (bare) and SA508 (oxidized) in accordance with (a) oxidation time and (b) contact angle.



**Figure 5. Surface change of bare and pre-oxidized (3 days) after nucleate boiling of 30 minutes ( $\times 60000$ , 500 nm).**

In Fig. 5, some differences of surface change between bare and pre-oxidized SA508 (3 days) are observed in terms of the existence of magnetite nanoparticles and whiskers. After nucleate boiling, unlike the bare SA508, the oxide products in pre-oxidized surface are almost grouped with closed-pores rather than forming the individual nanoparticles. It is because the remaining space on pre-oxidized surface disappears by water oxidation during boiling experiment, moreover, magnetite nanoparticles are no more formed on the free surface presumably due to lack of pure iron atoms. In addition, the whiskers on highly oxidized surface are almost removed during nucleate boiling. This means that adhesion force of whisker is too weak to maintain nanostructure on the surface, and then the effect of liquid spreading on the CHF seems to be vanished. Although wettability effect is reduced, it is doubtful why the CHF of the pre-oxidized SA508 is deteriorated in spite of maintaining hydrophilic behavior as ever. This unfavorable phenomenon cannot be explained by the hydrodynamic theory dealing with vapor-liquid interaction.

#### 4.2 Effect of thermal activity on oxide layer thickness

In the other point of view, surface aging effect concentrated on corrosion seems to be related to capability of heat dissipation near the CHF because the growth of oxide scale on metal surface constantly changes the thermal properties of effective surface. Based on thermal activity-based literatures, it has been revealed that the considerable change of thermal properties on the heating surface affects significantly to capability of heat conduction in the region where thermal gradient is high, i.e., dry spot [30, 31]. This effect is designated as a physical parameter of thermal activity,  $S$ , which is the product of the heater thickness,  $\delta$ , and the thermal effusivity,  $(\rho_h c_h k_h)^{0.5}$ , where  $\rho_h$  is the density,  $c_h$  is the specific heat capacity, and  $k_h$  is the thermal conductivity [31]. Thus, the CHF of the heating material, which has distinctive heater thicknesses and thermal properties, varies with thermal activity parameter. Bar-Cohen and McNeil proposed the asymptotic relationship between the CHF and the thermal activity with the fitting value  $C$  of 0.8 as follows [32]:

$$\frac{q_c''}{q_{c,asy}''} \propto \frac{S}{S + C} \quad (6)$$

where  $q_{c,asy}''$  is the asymptotic CHF, which indicates 90% of the maximum CHF. As a concern of the effect of highly effusive material on the CHF, moreover, Ahn et al. controlled the film thickness of graphene in the range from 15 to 200 nm. They also corrected the constant  $C$  in Eq. (6) with the range from 0.0001 to 0.001 because the thermal activity of the thin film in nanoscale was very low with the order of  $10^{-2}$  in spite of high thermal conductivity reaching to  $2000 \text{ W m}^{-1}\text{K}^{-1}$ . In other words, the fitting value is sensitive to the magnitude of thermal activity, and whose uncertainty is high in the range from 0 to 1. Noticeably, they confirmed the formation of local dry spot near the CHF using IR visualization [33]. Golobic and Bergles investigated the CHF variation with various ribbon heater with the range of thermal effusivity from 6000

to  $37000 \text{ J m}^{-2} \text{ K}^{-1} \text{ s}^{-1/2}$ . By controlling the heater thickness, moreover, they acquired the CHF data in terms of the thermal activity below 8. The CHF data above 300 points were fitted in nonlinear regression as a function of the thermal activity with the following relation [30]:

$$\frac{q_c''}{q_{c,asy}''} = 1 - e^{-(S/2.44)^{0.8498} - (S/2.44)^{0.0581}} \quad (7)$$

In connection with oxidation mechanism, it has been revealed that the oxidation behavior of metal is propagated from the free surface to inner bulk region. Since this reaction occurs electrochemically, the surface structure is deformed by the change of molecular composition from single components to ceramic series of iron oxide. Thus, the growth of oxide scale on the surface changes the physical and thermal properties within oxide layer.

**Table II. Thermal property of SS316, SA508, and iron oxide products**

	SS316	SA508	Magnetite	Hematite
Density ( $\text{kg m}^{-3}$ )	7960	7833	5175	5260
Specific heat capacity ( $\text{J kg}^{-1} \text{ K}^{-1}$ )	492	485	624	652
Thermal conductivity ( $\text{W m}^{-1} \text{ K}^{-1}$ )	14.7	40.8	3.7	5.9
Thermal effusivity ( $\text{J m}^{-2} \text{ K}^{-1} \text{ s}^{-1/2}$ )	7599	12453	3459	4500

Regarding the effect of thermal activity on the CHF, the thermal properties of the target surface have to be re-evaluated when pre-oxidized. Table II shows the thermal property of SS316, SA508, and oxide products, respectively. The thermal effusivity is the highest in the bare SA508, whereas those of oxide products decreased as lower thermal conductivity. Given that the upmost layer of pre-oxidized SA508 consists of magnetite only because hematite-based whiskers is practically swept out from the boiled surface (Fig. 5), the thermal effusivity of pre-oxidized surface is lower than that of SA508 by 0.28 times. Similarly, in flow boiling CHF experiment for evaluating material effect of the SA508, Part et al. insisted that hematite-based layer formed on the upmost surface of the SA508 is easily removed in flow boiling condition, finally magnetite becomes the outer surface layer [28].

**Table III. Change of thermal activity along oxidation time**

	3 days	10 days	20 days	30 days	40 days
Estimated oxide layer thickness ( $\mu\text{m}$ )	0.30	0.58	0.88	0.95	1.12
Thermal activity ( $\text{J m}^{-1} \text{ K}^{-1} \text{ s}^{-1/2} \times 10^{-3}$ )	1.03	2.00	3.04	3.27	3.88

As confirmed in Fig. 1(b), the oxide scale being the effective boiled surface has grown in the range of hundreds of nanoscale, whose layer is very thin compared to the heater thickness of 2 mm. By using both parameters, the thermal activity of pre-oxidized SA508 was calculated and summarized in Table III. In a distinctive two nanoscale layers, determining the thermal activity only using the thin upmost layer might be uncertain to validate its effect on the CHF. It is because defining the effective heater thickness in a

composite layer will be challenging. For example, the heat dissipation mechanism on the boiling surface can be affected by the thermal properties of SA508 sublayer even though the upmost layer regarded as the effective thickness consists of a series of oxide products, which are apparently distinctive to the sublayer. As a relevant study in terms of heating thickness in nanoscale, Ahn et al. investigated the effect of thermal activity of graphene film, whose heating substrate is a silicon wafer, on the CHF. Although the graphene film was deposited on the silicon substrate in nanoscale, the highly conductive graphene enhanced the CHF gradually until the thickness of graphene film reaches to 150 nm [33]. Thus, it is also expected that magnetite-based nanolayer becomes the effective layer responsible for determining the amounts of heat dissipation near the CHF.

The CHF data of pre-oxidized SA508 as a non-dimensional form of the measured CHF over the maximum CHF are plotted with the thermal activity-based CHF correlations in Fig. 6. In this study, the maximum CHF value corresponding to the asymptotic line was not found because simulating the thick-oxide layer manufacturing microscale oxidation requires infeasible time of months or years under the thermal state of the RPV and thus is impractical in the laboratory system. Instead, the maximum CHF value may be defined by the surface parameters of bulk oxide (i.e. wettability, roughness, and capillarity). Since the pre-oxidized surface of SA508 is non-rough and non-porous, wettability is to be only a deterministic factor to the CHF. Accordingly, based on Eq. (5), the maximum CHF value was calculated as 1348 kW/m<sup>2</sup> with the contact angle of 40°.

The present CHF data are barely comparable with the proposed CHF correlations in the range of  $0 < S < 1$  (Fig. 6(a)). However as the range of  $S$  is focused on the range of  $0 < S < 0.01$ , a dependency of  $S$  on the non-dimensional CHF becomes clarified with help of empirical correlations of Golobic and Bergles. Moreover, in Eq. (6), the optional fitting value  $C$  was suggested by Ahn et al. (Fig. 6(b)). Definitely, it is involved with the range of the effective heater thickness. Golobic and Bergles assigned the minimum heater thickness as 5 μm corresponding to the  $S$  value of 0.045 [30]. Furthermore, the heater thickness of nanoscale is used in highly effusive material of graphene oxide in the range of  $0.001 < S < 0.01$ , which includes the  $S$  value of the present data [33]. As shown in Fig. 6(b), the present CHF data are higher than the estimated CHF by Eq. (7) with the maximum relative error of 23%, and also following the fitting lines of Ahn et al.'s prediction. However, the increasing trend with respect to the  $S$  value is not observed. It is because the range of the oxide layer thickness is too narrow to characterize the effect of thermal activity on the CHF. In order to identify the relationship between the thermal activity and the CHF, the thicker oxide layer in the range of dozens of micrometers has to be simulated. Nevertheless, the reason for deterioration of the CHF of pre-oxidized SA508 can be explained by the thermal activity-based theory.

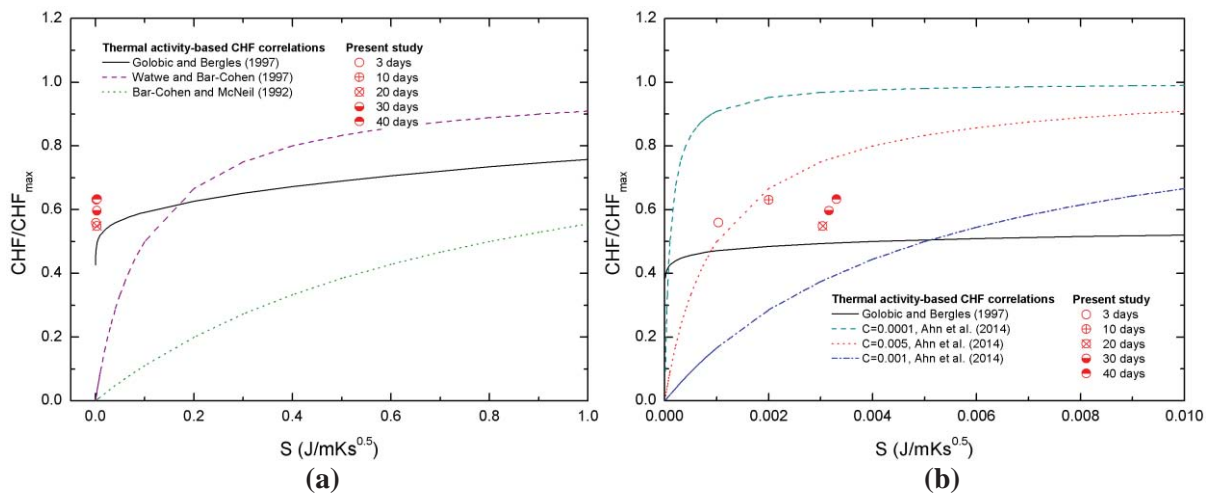


**Figure 6. CHF variation of the pre-oxidized SA508 with the thermal activity-based CHF correlations in range from (a) 0 to 1 and (b) 0 to 0.01.**

## 5. SUMMARY AND CONCLUSIONS

In this study, pool boiling CHF experiment was conducted to evaluate the effect of pre-oxidation of the SA508 on the CHF. After air oxidation in 300 °C, the oxide structure composed mainly of Fe and O was formed on the surface. The growth of oxide scale followed the parabolic rate law, and the oxide layer thickness was estimated by measuring the mass gain in each oxidation time. Major findings are summarized as follows:

- (1) As air oxidation continues, the contact angle decreased gradually with the increase of surface free energy and roughness. After 30 days, the liquid spreading effect was observed in contact angle measurement due to the enhanced capillarity with the presence of whiskers. However, the whiskers were swept out from the boiled surface, which, in turn, changed the contact angle to increase. Nevertheless, it is still lower than 67° of the bare SA508.
- (2) In the bare SA508, the nano-porous structure made of magnetite nanoparticles were formed on the heating surface during nucleate boiling of 30 minutes. Although the contact angle was almost the same regardless of surface change, the presence of nano-porous structure enhanced the CHF by approximately 1.5 times.
- (3) The CHF of the pre-oxidized SA508 was deteriorated by 0.65 times compared to Zuber's CHF value even though the surface is hydrophilic. Unlike the bare SA508, a porous structure was hardly developed on the pre-oxidized surface during nucleate boiling. Given that the thermal effusivity of magnetite was lower by 0.28 times than the bare SA508 and the crystallized oxide layer grew continuously in micro/nanoscale according to the parabolic rate law, it is due to reduced thermal activity with the order of  $10^{-3}$ . Thus, it weakens the capability of heat dissipation toward lateral side subsequent to cause local dry spot.

## ACKNOWLEDGMENTS

This research was supported by National R&D Program through the National Research Foundation of Korea (NRF) funded by the Korean Government (MSIP) (No. 2012M2B2A6029184).

## REFERENCES

1. T.G. Theofanous, C. Liu, S. Additon, S. Angelini, O. Kymäläinen and T. Salmassi, "In-vessel coolability and retention of a core melt," *Nucl. Eng. Des.* **169**(1–3), pp. 1-48 (1997).
2. T.G. Theofanous, S. Syri, T. Salmassi, O. Kymäläinen and H. Tuomisto, "Critical heat flux through curved, downward facing, thick walls," *Nucl. Eng. Des.* **151**(1), pp. 247-258 (1994).
3. F.B. Cheung and K.H. Haddad, "A hydrodynamic critical heat flux model for saturated pool boiling on a downward facing curved heating surface," *Int. J. Heat Mass Transf.* **40**(6), pp. 1291-1302 (1997).
4. R. Park, K. Kang, S. Hong, S. Kim and J. Song, "Corium behavior in the lower plenum of the reactor vessel under IVR-ERVC condition: technical issues," *Nucl. Eng. Technol.* **44**(3), pp. 237-248 (2012).
5. S. Chol, "Enhancing thermal conductivity of fluids with nanoparticles," *ASME-Publications-Fed* **231**, pp. 99-106 (1995).
6. S. Kim, I. Bang, J. Buongiorno and L. Hu, "Surface wettability change during pool boiling of nanofluids and its effect on critical heat flux," *Int. J. Heat Mass Transf.* **50**(19), pp. 4105-4116 (2007).
7. H.D. Kim and M.H. Kim, "Effect of nanoparticle deposition on capillary wicking that influences the critical heat flux in nanofluids," *Appl. Phys. Lett.* **91**(1), p. 014104 (2007).
8. J. Yang, M. Dizon, F. Cheung, J. Rempe, K. Suh and S. Kim, "CHF enhancement by vessel coating for external reactor vessel cooling," *Nucl. Eng. Des.* **236**(10), pp. 1089-1098 (2006).
9. G.H. Seo, H. Hwang, J. Yoon, T. Yeo, H.H. Son, U. Jeong, G. Jeun, W. Choi and S.J. Kim, "Enhanced critical heat flux with single-walled carbon nanotubes bonded on metal surfaces," *Exp. Therm. Fluid Sci.* **60**, pp. 138-147 (2015).

10. J. Lee and S.H. Chang, "An experimental study on CHF in pool boiling system with SA508 test heater under atmospheric pressure," *Nucl. Eng. Des.* **250**, pp. 720-724 (2012).
11. G. DeWitt, R. Park, J. Buongiorno, T. McKrell and L. Hu, "Investigation of Downward Facing CHF with Water-Based Nanofluids for IVR," Ph.D. Thesis, Boston (2011).
12. B.D. Craig and D.S. Anderson, *Handbook of corrosion data*, ASM international, (1994).
13. H. Sakai, T. Tsuji and K. Naito, "Oxidation of Iron in Air between 523 and 673 K," *J. Nucl. Sci. Technol.* **22**(2), pp. 158-161 (1985).
14. N. Bertrand, C. Desgranges, D. Poquillon, M.C. Lafont and D. Monceau, "Iron Oxidation at Low Temperature (260-500 A degrees C) in Air and the Effect of Water Vapor," *Oxidation of Metals* **73**(1-2), pp. 139-162 (2010).
15. R.M. Cornell and U. Schwertmann, *The Iron Oxides.*, VCH, Weinheim, Germany (1996).
16. A. Fry, S. Osgerby and M. Wright, *Oxidation of Alloys in Steam Environments: A Review*, National Physical Laboratory Middlesex, (2002).
17. R.J. Hussey, G.I. Sproule, D. Caplan and M.J. Graham, "The growth and structure of oxide films formed on Fe in O<sub>2</sub> and CO<sub>2</sub> at 550°C," *Oxidation of Metals* **11**(2), pp. 65-79 (1977).
18. H.S. Ahn, C. Lee, H. Kim, H. Jo, S. Kang, J. Kim, J. Shin and M.H. Kim, "Pool boiling CHF enhancement by micro/nanoscale modification of zircaloy-4 surface," *Nucl. Eng. Des.* **240**(10), pp. 3350-3360 (2010).
19. H. O'Hanley, C. Coyle, J. Buongiorno, T. McKrell, L.-W. Hu, M. Rubner and R. Cohen, "Separate effects of surface roughness, wettability, and porosity on the boiling critical heat flux," *Appl. Phys. Lett.* **103**(2), 024102 (2013).
20. S. Li, J. Cai, Y. Mei, Y. Ren and G. Qin, "Thermal Oxidation Preparation of Doped Hematite Thin Films for Photoelectrochemical Water Splitting," *International Journal of Photoenergy*, **2014** (2014).
21. S.G. Kandlikar, "A Theoretical Model to Predict Pool Boiling CHF Incorporating Effects of Contact Angle and Orientation," *J. Heat Transf.-Trans. ASME* **123**(6), pp. 1071-1079 (2001).
22. R.N. Wenzel, "RESISTANCE OF SOLID SURFACES TO WETTING BY WATER," *Industrial & Engineering Chemistry* **28**(8), pp. 988-994 (1936).
23. A.B.D. Cassie and S. Baxter, "Wettability of porous surfaces," *Transactions of the Faraday Society* **40**(0), pp. 546-551 (1944).
24. S.A. Gomez-Lopera, R.C. Plaza and A.V. Delgado, "Synthesis and characterization of spherical magnetite/biodegradable polymer composite particles," *Journal of Colloid and Interface Science* **240**(1), pp. 40-47 (2001).
25. Y. Oshida, R. Sachdeva and S. Miyazaki, "Changes in contact angles as a function of time on some pre-oxidized biomaterials," *J Mater Sci: Mater Med* **3**(4), pp. 306-312 (1992).
26. M.-G. Kang, "Effect of surface roughness on pool boiling heat transfer," *Int. J. Heat Mass Transf.* **43**(22), pp. 4073-4085 (2000).
27. N. Zuber, "Hydrodynamic aspects of boiling heat transfer," Ph.D. Thesis, Los Angeles, CA (1959).
28. H.M. Park, Y.H. Jeong and S. Heo, "Effect of heater material and coolant additives on CHF for a downward facing curved surface," *Nucl. Eng. Des.* **278**, pp. 344-351 (2014).
29. G.R. Beitel, "Boiling Heat-Transfer Processes and Their Application in the Cooling of High Heat Flux Devices," 152 (1993).
30. I. Golobic and A.E. Bergles, "Effects of heater-side factors on the saturated pool boiling critical heat flux," *Exp. Therm. Fluid Sci.* **15**(1), pp. 43-51 (1997).
31. M. Arik and A. Bar-Cohen, "Effusivity-based correlation of surface property effects in pool boiling CHF of dielectric liquids," *Int. J. Heat Mass Transf.* **46**(20), pp. 3755-3764 (2003).
32. A. Bar-Cohen and A. McNeil, "Parametric effects on pool boiling critical heat flux in highly wetting liquids," in: *Proceedings of Engineering Foundation Conference on Pool and External Flow Boiling*, pp. 171-176 (1992).
33. H.S. Ahn, J.M. Kim, T. Kim, S.C. Park, J.M. Kim, Y. Park, D.I. Yu, K.W. Hwang, H. Jo, H.S. Park, H. Kim and M.H. Kim, "Enhanced heat transfer is dependent on thickness of graphene films: the heat dissipation during boiling," *Scientific Reports* **4** (2014).